# Ultraviolet and Visible Reflectance Spectra of Phobos and Deimos as Measured by the ExoMars-TGO/NOMAD-UVIS Spectrometer

J. P. Mason[1] , M. R. Patel[1,2] , M. Pajola[3] , E. D. Cloutis[4] , J. Alday[1,5] , K. S. Olsen[6] , C. Marriner[1], J. A. Holmes[1] , G. Sellers[1], N. Thomas[7], M. Almeida[7], M. Read[7], H. Nakagawa[8] , I. R. Thomas[9] , B. Ristic[9] , Y. Willame[9], C. Depiesse[9] , F. Daerden[9] , A. C. Vandaele[9] , J. J. Lopez-Moreno[10], and G. Bellucci[11]

[1]School of Physical Sciences, The Open University, Milton Keynes, UK, [2]Space Science and Technology Department, Science and Technology Facilities Council (STFC), Rutherford Appleton Laboratory, Didcot, UK, [3]Osservatorio Astronomico di Padova, Istituto nazionale di astrofisica (INAF), Padua, Italy, [4]Centre for Terrestrial and Planetary Exploration, University of Winnipeg, Winnipeg, MB, Canada, [5]Graduate School of Frontier Sciences, University of Tokyo, Kashiwa, Japan, [6]Department of Physics, University of Oxford, Oxford, UK, [7]Space Research and Planetology Division, Physikalisches Institut, Universität Bern, Bern, Switzerland, [8]Tohoku University, Sendai, Japan, [9]Royal Belgian Institute for Space Aeronomy (BIRA-IASB), Brussels, Belgium, [10]Instituto de Astrofisica de Andalucía (IAA), Consejo Superior de Investigaciones Científicas (CSIC), Granada, Spain, [11]Istituto di Astrofisica e Planetologia Spaziali, INAF, Rome, Italy

**Abstract** Spectroscopic measurements are a powerful tool to investigate the surface composition of airless bodies and provide clues of their origin. The composition and origin of Phobos and Deimos are still unknown and are currently widely debated. We present spectroscopic measurements of Phobos and Deimos at ultraviolet and visible wavelengths (250–650 nm) made by the NOMAD-Ultraviolet and Visible Spectrometer (UVIS) on the ExoMars TGO mission. These new spectra cover multiple areas on Phobos and Deimos, and are of generally higher spectral resolution and signal-to-noise than previous spectra, and extend to lower wavelengths than most previous measurements. The UVIS spectra confirm a red-sloped spectrum lacking any strong absorption features; however, we confirm the presence of a previously identified absorption feature near 0.65 μm and tentative absorption near 0.45 μm. The observed Phobos and Deimos spectra are similar to D- and T-type asteroids, adding weight to the captured asteroid hypothesis for the moons' origins. We also find, however, that the UVIS Phobos reflectance spectra of Phobos' red unit is a relatively close match to the olivine-rich, highly shocked Mars meteorite NWA 2737, with a low overall reflectance, a red-sloped spectrum, and lack of olivine-associated absorption bands in the UVIS spectral range. This meteorite, however, exhibits spectral features at longer wavelengths that not observed in the Martian moon spectra, indicating a need for further investigation at longer wavelengths to interpret whether this material could inform our understanding of Phobos' origin.

**Plain Language Summary** Whether the Martian moons Phobos and Deimos are captured asteroids that originated outside the Mars system or formed from a debris disk around Mars during its formation or following a large impact on Mars is widely debated. Measurements of reflected sunlight from the surfaces of Phobos and Deimos can provide pivotal information on their composition as well as clues to their origins. In this study, we present a comparison between observations of Phobos and Deimos made with the NOMAD Ultraviolet and VIsible Spectrometer (UVIS) on the ExoMars Trace Gas Orbiter (TGO) and previous spectral measurements from other missions. The UVIS spectra show a good agreement with previous observations, with the Phobos and Deimos spectra showing a red-sloped spectrum similar to primitive carbonaceous chondrite asteroids. A change in the spectral slope at wavelengths longer than 0.53 μm is shown to be consistent with the previously identified 0.65 μm absorption feature. The similarity between the measured Phobos ultraviolet and visible spectrum and highly-shocked olivine from the Mars meteorite NWA 2737 entices the question of whether Phobos and Deimos surfaces could be composed of a similar dark olivine matrix and formed within the accretion disk created from a giant impact on Mars.

## 1. Introduction

The origin of Phobos and Deimos is still unknown, with the two leading hypotheses being as a captured, possibly primitive carbonaceous chondrite, asteroid, or from accretion within a debris disk following a giant impact on Mars. The spectral, and visual, likeness of Phobos and Deimos to primitive carbonaceous chondrite asteroids

led to the proposition of the moons being captured asteroids (Bell et al., 1993; Burns, 1978, 1992; Murchie et al., 1991; Pollack et al., 1979; Thomas et al., 1992) and more recent observations have continued to show the spectral similarity between the moons and D-type and T-type asteroids (Fraeman et al., 2014; Murchie & Erard, 1996; Pajola et al., 2013). The captured asteroid theory, however, fails to account for the near-circular orbit of the martian moons. Pajola et al. (2012) proposed an updated collisional scenario for the capture of Phobos and showed that the capture of a D-type asteroid ejected from the main asteroid belt could be possible following a collision with a planetesimal in the martian orbital vicinity.

The origin of Phobos and Deimos from accretion within a debris disk, following a giant impact on Mars was proposed by Craddock (1994, 2011) and more recent studies have shown that such a formation mechanism can explain the orbital characteristics of both moons, but not their spectral properties (Hesselbrock & Minton, 2017; Hyodo & Charnoz, 2017; Hyodo & Ohtsuki, 2015; Ida et al., 1997; Rosenblatt et al., 2016). Ronnet et al. (2016) showed that direct gas-to-solid condensation in the outer edges of the debris disk could lead to the creation of small ($<2\ \mu m$) sized particles and that the accretion of such small particles, as the building blocks of Phobos and Deimos, could explain both their physical and spectral characteristics.

Neither the captured asteroid nor the accretion scenario can fully reconcile the orbital, physical and spectral properties of Phobos and Deimos. High-resolution spectral measurements can help answer the origin question of the moons by identifying absorption bands associated with various transition series elements, including spin-forbidden and charge-transfer bands, in order to constrain possible surface mineralogy.

The first spectral measurements of Phobos and Deimos by the Mariner 9 and Viking missions showed the moons to have a dark and flat visible spectrum analogous to low-albedo C-type asteroids (Pang et al., 1978, 1983; Pollack et al., 1978). Later spectral measurements in the ultraviolet (UV) through to the near-infrared (NIR) by the Combined Photometer and radiometer for Mars (KRFM) and the Imaging Spectrometer for Mars (ISM) aboard Phobos 2 (Murchie & Erard, 1996) showed that Phobos and Deimos exhibited a dark red-sloped spectrum (i.e., the reflectance increases with increasing wavelength) inconsistent with C-type asteroids and more analogous to D-type to T-type asteroids. Furthermore, the Phobos 2 observations revealed that the surface of Phobos contained two distinct geographic units that differed in their color and UV spectral properties. The "blue unit" is associated with the interior and ejecta of the Stickney crater (the largest crater on Phobos, with a size of 9 km) and is predominantly located in the Phobos leading hemisphere. On the contrary, the "red unit" covers the rest of the surface and dominates the Phobos trailing hemisphere (Murchie et al., 1991). The boundary between the blue and red units in the sub-Mars hemisphere (i.e., the hemisphere of the moon that faces Mars) is unknown but has been estimated to be near the sub-Mars point (the location on the moon's surface that a vector joining the center of Mars to the center of Phobos would intersect) (Murchie et al., 1999; Pajola et al., 2017). Spectrally, the reflectance of the blue unit exhibits a flatter red-sloped gradient compared to the red unit, which shows greater drop off at wavelengths shorter than 400 nm. The Phobos leading edge was measured using the Hubble Space Telescope (HST) Faint Object Spectrograph (FOS) (Zellner & Wells, 1994), with the resultant spectrum consistent with the shallower red-sloped Phobos blue unit revealed from the Phobos 2 measurements (Murchie & Erard, 1996). The Imager for Mars Pathfinder (IMP) provided spectral measurements of the sub-Mars hemisphere, which was shown to have spectral characteristics intermediate between the blue and red units. However, a closer resemblance to the red unit suggests that the sub-Mars hemisphere is dominated by the red unit (Murchie et al., 1999). The IMP measurements also provided the first evidence of a weak spectral feature in the Phobos spectrum between 600 and 700 nm. This weak 650 nm feature was later confirmed by telescopic measurements of Phobos (Binzel et al., 2001, 2004) and showed the band depth increased with increasing distance from the blue unit.

More recent observations made using the Observatoire pour la Minéralogie, l'Eau, les Glaces et l'Activité (OMEGA) aboard Mars Express (Bibring et al., 2004) and the Compact Reconnaissance Imaging Spectrometer for Mars (CRISM) on the Mars Reconnaissance Orbiter (Murchie et al., 2007) refined our knowledge of the dark, nearly featureless, red-sloped spectrum of Phobos from visible to NIR wavelengths. The images taken by OMEGA and CRISM allowed for a direct comparison of the Phobos red and blue units, confirming a flatter spectrum for the former (Fraeman et al., 2012; Pajola et al., 2018). In addition, the CRISM measurements provided further confirmation of the weak spectral feature centered around 0.65 μm, revealing band depths between 1% and 4% for the Phobos red unit and no absorption seen for the blue unit (Fraeman et al., 2014). Disc-integrated measurements

of the Phobos trailing edge were obtained by the Optical, Spectroscopic, and Infrared Remote Imaging System (OSIRIS) on Rosetta (Keller et al., 2007). The OSIRIS spectrum was in good agreement with previous observations, with a steeper UV drop off indicative of the red unit (Pajola et al., 2012).

While Deimos has not been as extensively observed as Phobos, spectroscopic observations of Deimos have been performed using the HST FOS (Zellner & Wells, 1994), Mars Pathfinder (Murchie et al., 1999) and CRISM (Fraeman et al., 2012). These observations have shown that Deimos exhibits a red-sloped reflectance spectrum at UV and visible wavelengths similar to the Phobos red unit (Pang et al., 1978, 1983; Pollack et al., 1978). While this similarity between the spectral reflectance of Deimos and Phobos' red unit could suggest a common origin for both moons, the surface of Deimos is more spectrally uniform and does not display distinct spectral units (Pang et al., 1983; Rivkin et al., 2002).

Potential absorption at 0.65 μm is the only identified spectral feature at UV and visible wavelengths in the Phobos and Deimos spectra and is a common feature observed on red, low albedo primitive asteroids (Chapman et al., 1973). The likeness of the surface reflectance of Phobos and Deimos to primitive D-type and T-type asteroids (Fraeman et al., 2012; Murchie & Erard, 1996; Pajola et al., 2012; Rivkin et al., 2002) provides supportive evidence that Phobos and Deimos could be captured asteroids. Furthermore, a 0.65 μm spectral feature is not readily diagnostic of a specific mineralogy and therefore insufficient to determine the mineralogy of the moons. Fraeman et al. (2014) have shown that the 0.65 μm feature can be sufficiently replicated by highly desiccated Fe-phyllosilicates or by nanophase Fe-particles ranging from a few nanometers to a few micrometers in size that could arise from space-weathering-related processes, resulting in the formation of Fe and OH on the moons' surfaces, similar to lunar mare soils found on Earth's Moon as a product of space weathering (Clark et al., 2012; Pieters et al., 2000).

The NOMAD-UVIS results presented in this paper arguably provided the highest quality reflectance spectra in the 250–650 nm region. UVIS provides the opportunity to verify previous observations of possible spectral features and to search for absorption bands associated with various transition series elements, including spin-forbidden and charge-transfer bands (e.g., Cloutis, 1997, 2002; Greenberger et al., 2015). Spin-forbidden bands can be narrow, on the order of a few to a few tens of nanometers, and can indicate the presence, crystallographic structure, and oxidation state of specific cations. However, such narrow absorption bands could be missed by multispectral imagers or could be confused with noise in the higher spectral resolution, lower signal to noise data. We can use previous observations in this and other wavelength regions to constrain possible surface mineralogy (such a review was recently presented by Poggiali et al. (2022)) and investigate the implications of these observations in providing new information about the origin of the martian moons. In Section 2, we present the UVIS observations and their main characteristics and Section 3 describes the calibration process. Finally, in Section 4, we present the characteristics of the spectral reflectance of Phobos and Deimos at the UVIS wavelengths and discuss the implications of these new measurements.

## 2. UVIS Observation Characteristics

UVIS is the UV-Vis channel of the Nadir and Occultation for MArs Discovery (NOMAD) spectrometer suite (Vandaele et al., 2018) aboard the ExoMars Trace Gas Orbiter (TGO) and has been operating in Mars orbit since April 2018. A full description of the UVIS instrument and its calibration can be found in Patel et al. (2017), Mason et al. (2022), and Willame et al. (2022). UVIS has been performing approximately two to three measurement campaigns of the martian moons every month since September 2021, with each campaign containing between 45 and 120 separate spectral measurements, called frames.

The apparent size of Phobos in the UVIS Field of View (FOV) ranges from a minimum of just under 11.8 arcminutes to a maximum of 13.7 arcminutes. This is significantly smaller than the UVIS nadir FOV of 43 arcminutes, therefore, Phobos does not fill the entire FOV of the UVIS nadir channel. However, the total nadir FOV is formed of 19 optical fibers which individually have an angular FOV of ~7 arcminutes (Patel et al., 2017), allowing Phobos to fill the FOV of a single fiber. In Figure 1a, we provide an illustration of the UVIS FOV with the 19 optical fibers superimposed on Phobos for the UVIS measurement campaign performed on 16 October 2022. The image of Phobos was generated using the NASA Navigation and Ancillary Information Facility (NAIF) SPICE toolkit (Acton, 1996; Acton et al., 2018) (hereafter referred to simply as SPICE). Approximately 11 min after
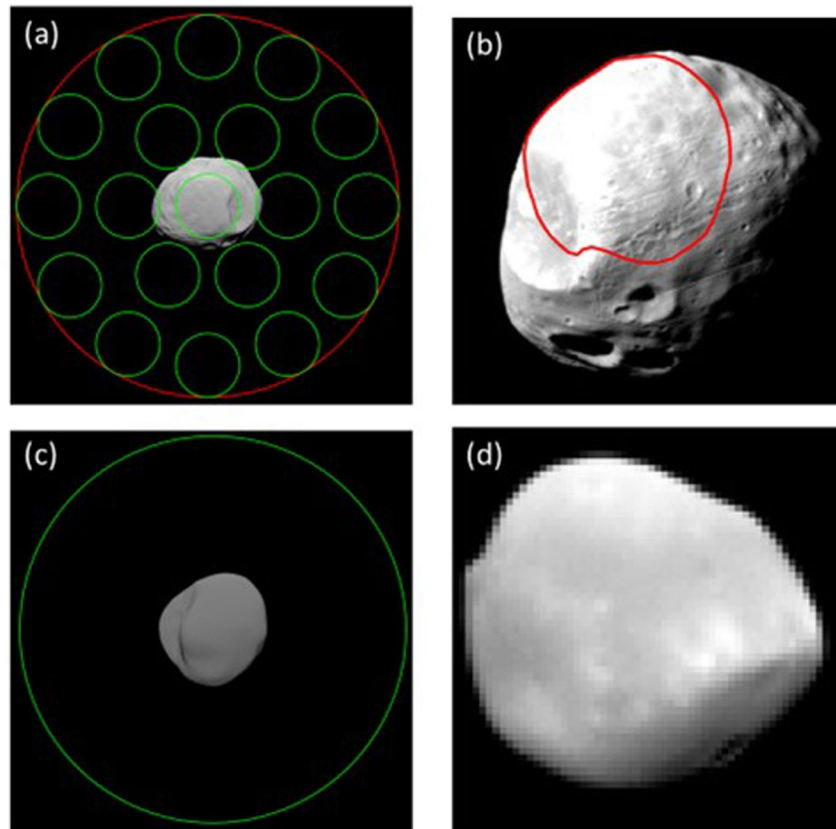
**Figure 1.** (a) An illustration of the UVIS Phobos measurement taken on 16 October 2022 showing the size of Phobos compared to the FOV of the nadir channel (red circle) and the FOV of the individual fibers (green circles). (b) CaSSIS image of Phobos taken 11 min after the UVIS measurement. The red footprint shows the projection of a UVIS fiber FOV on the surface of Phobos. (c) An illustration of the size of Deimos compared to the FOV of a single fiber (green circle) for the observation made on 25 October 2022. (d) CaSSIS image of Deimos taken on 4 September 2022 to provide context for the hemisphere of Deimos measured by UVIS.

this UVIS observation, an image of Phobos was captured (Figure 1b) by the Color and Stereo Surface Imaging System (CaSSIS) (Roloff et al., 2017; Thomas et al., 2017, 2022) aboard TGO, providing context for the projection of UVIS FOV on the surface of Phobos. Since the apparent size of Phobos is comparable to the individual fiber FOV, the resulting spectra can be regarded as disc-integrated measurements. The two Phobos campaigns we present in this study were executed on 28 May 2022 (here after May-22) and 16 October 2022 (Oct-22) and were chosen as the best candidates for representing the red and blue units on the surface of Phobos. The interested reader can find the spectra from all UVIS Phobos observations in Appendix A.

The apparent size of Deimos in the nadir FOV is significantly smaller than the FOV of a single fiber, with an apparent diameter of approximately 2 arcminutes. As such, all measurements of Deimos are disc-integrated. Deimos observations with mid-to-high phase angles have low signal-to-noise ratios (SNR) <4 that limit any useful analysis. The single campaign we present in this study was performed on 25 October 2022 and represents the optimal Deimos measurement by UVIS to date. The observations during this campaign had a mean phase angle of ~28° with a minimum of ~10° at the start of the observation, a SNR of ~14 at 260 nm and a SNR of >60 across visible wavelengths. Figure 1c shows the simulated projection of Deimos generated using SPICE within the FOV of a single fiber (green circle) and Figure 1d shows a CaSSIS image of Deimos taken on 4 September 2022 to provide context for the sub-Mars hemisphere of Deimos.

For Phobos and Deimos observations, UVIS is pointed along the vector from TGO to the center of moons. Since Phobos and Deimos are tidally locked and the orbit of TGO lies within the orbit of Phobos, UVIS always observes the same general area (with only slight deviations), which is located east of Stickney Crater in the sub-Mars

hemisphere. It is important to highlight that the UVIS measurement campaigns are always performed when TGO is on the nightside of Mars; therefore, we do not have to consider Mars-shine in our calculated reflectance factor (defined as the measured radiance divided by the incident solar irradiance).

Spacecraft constraints prohibited tracking of a specific location on the surface; therefore, each individual observation within a measurement campaign will observe a slightly different location on the surface as Phobos rotates with respect to the FOV. The phase angle also varies during a campaign as TGO moves along its orbit, with the amount of signal received by UVIS decreasing as the phase angle increases, reducing the SNR. To limit the introduction of increased noise from measurements at higher phase angles, and to reduce any spatial variability in our spectrum, we averaged all frames containing a signal intensity greater than 90% of the maximum signal observed throughout the Phobos pass and constrain the change in observed position on the surface to $\pm 1°$. With these criteria, 7 and 16 frames are combined to produce a single Phobos observation spectrum for each measurement campaign.

The two Phobos observations we present here cover slightly different geographical locations on Phobos, which we illustrate in Figures 2a and 2b. The outlines in Figures 2a and 2b represent the projected footprint of the central UVIS fiber FOV superimposed on the Viking Phobos mosaic (Simonelli et al., 1993; Stooke, 2015) and the illumination was calculated using SPICE for the time of peak signal recorded by UVIS. All observations are centered near the sub-Mars point with observation Oct-22 (Figure 2b) being the furthest offset toward Stickney crater, while observation May-22 (Figure 2a) is centered southeast of the sub-Mars point. Figure 2c shows the Viking mosaic of Deimos modified to show the illumination at the time of the UVIS Deimos observation. Since the FOV is larger than Deimos, we illustrate what UVIS observed by only showing surface regions that were visible to UVIS (setting any surface segment with a phase angle $>90°$, calculated using SPICE, to black).

## 3. Data Reduction and Calibration

During the nominal operation observing the martian atmosphere, all 19 fibers are usually illuminated within the nadir FOV. The light from each fiber is projected onto a different CCD row along the detector $y$-axis, while the spectral information is projected across the CCD columns along the detector $x$-axis (see Figure 1 in Mason et al., 2022). Since Phobos does not fill the total UVIS FOV, only a couple of fibers will be illuminated and the distribution of light on the detector will differ from that of a typical Mars nadir observation. The light dispersion on the UVIS detector for a single frame in a Phobos observation, showing three fibers illuminated, is shown in Figure 3. The first thing to note is that, compared to the Mars' nadir-viewing observations (Mason et al., 2022), no straylight is evident in the Phobos frame. The source of the straylight within UVIS is not fully understood; however, the lack of straylight in the Phobos and Deimos observation points toward the source of the straylight perhaps arising from the outer optical fibers positioned away from the central axis of the spectrometer mirrors, resulting in internal scattering.

The calibration procedure begins by dividing the CCD frame into two regions, the first region contains the two fibers between CCD rows 50 and 109 (since their signals overlap and merge at longer wavelengths), and a second region that contains a third illuminated fiber centered at row 120 (see Figure 3a). The signal through the third fiber is extremely weak and therefore the second region is discarded. Before we can process an observation, the illuminated region on the CCD frame must be determined. To do this, we reduce the resolution of the frame using binning the pixels in the spectral direction creating 32 spectral bins, this has the advantage of making the boundary between non-illuminated and illuminated pixels more distinct. The width of the illuminated region for each binned column is found by taking the gradient of the signal across the binned column and looking for the first pixel to have a negative gradient, starting from the pixel with the peak signal and moving toward the readout register. Similarly, the trailing edge of the dispersion is found by looking for the first positive gradient after the peak signal in the second fiber. The bounds for the coarse resolution frame are then interpolated back to the UVIS full-wavelength resolution.

The data processing follows a similar method to that used for the UVIS solar occultation and nadir channels for visible wavelengths >526 nm (Mason et al., 2022; Willame et al., 2022). After the electronic offset, bright pixel and dark current removal, a second order polynomial is fitted either side of the illuminated region to remove any residual signal. The corrected Phobos frame along a single column is shown in Figure 3b for
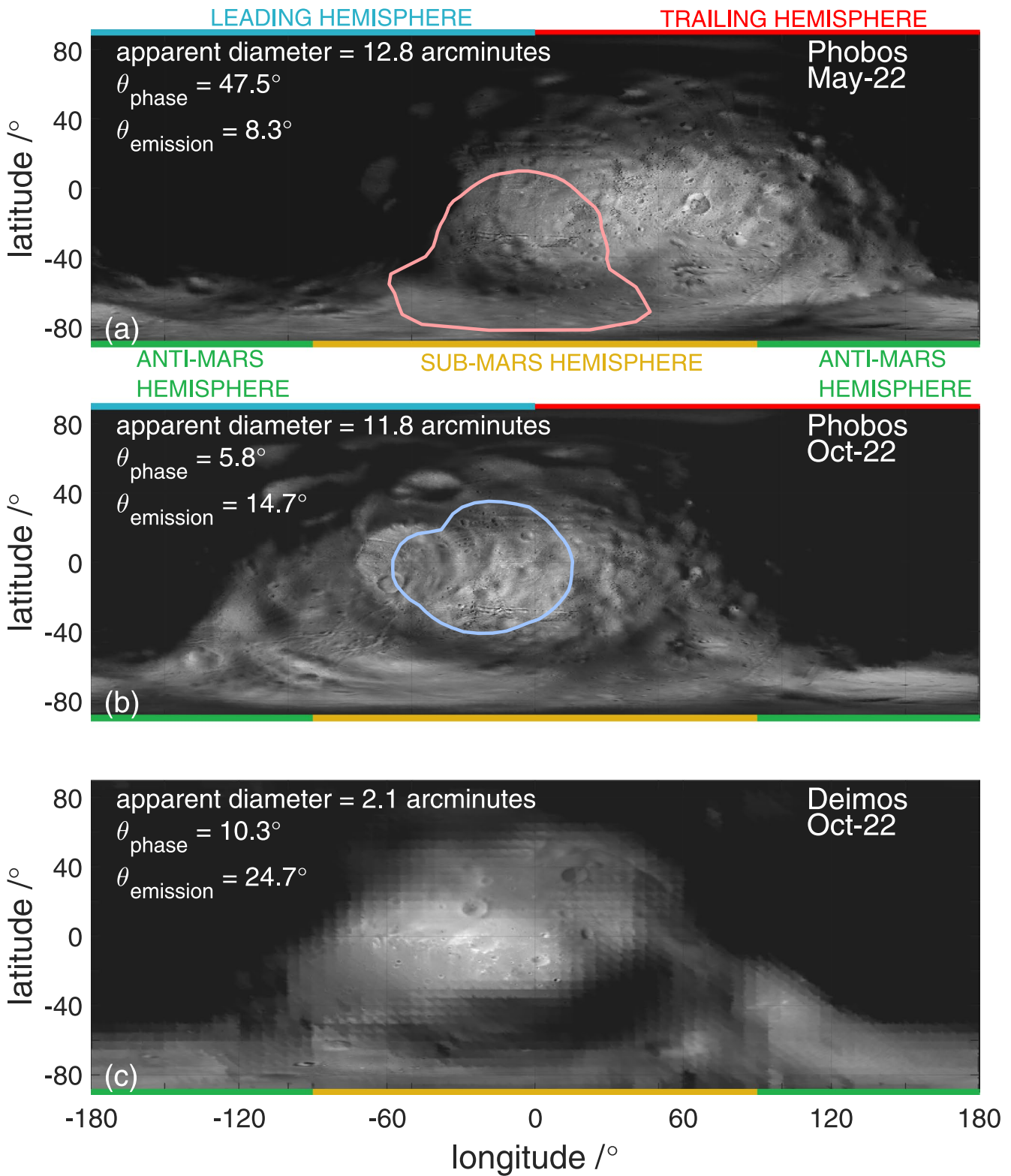
**Figure 2.** Panels (a, b) show the projected footprint of the central fiber on the Phobos surface for observations taken on 28 May 2022 (May-22) and 16 October 2022 (Oct-22) superimposed on the Viking mosaic of Phobos. Panel (c) shows the illumination of the Deimos surface for the Deimos observation superimposed on the Deimos Mosaic produced by Viking. As described in the main text, the surface illumination of Phobos and Deimos at the time of the UVIS observation was calculated using SPICE.
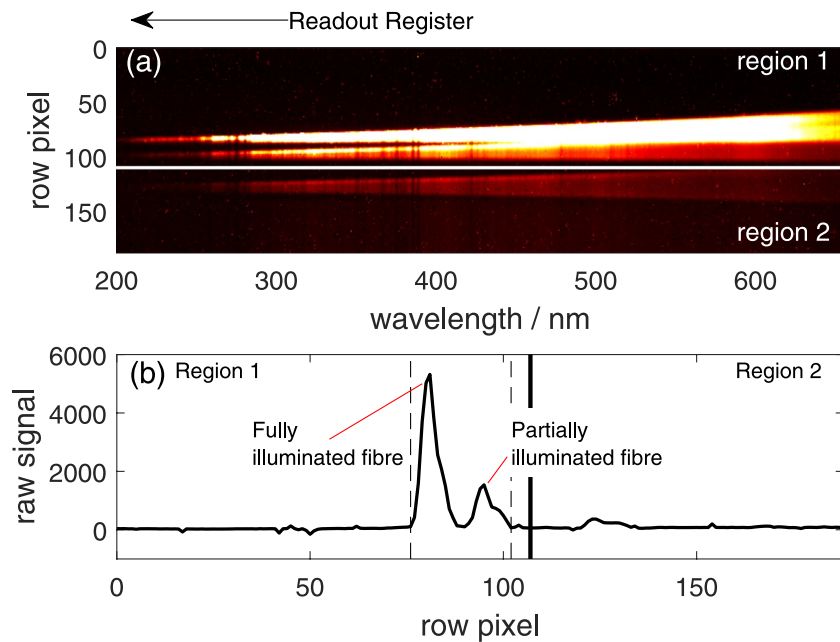
**Figure 3.** (a) Example of the raw output on the UVIS detector array during a Phobos observation. Region 1 contains the signal of two fully and partially illuminated fibers, respectively, that are combined to produce the Phobos spectrum. Region 2 contains a single fiber that is only faintly illuminated with a very low signal that is not included in the creation of the final spectrum. Panel (b) shows the dispersion of light down column pixel 238 (310 nm), showing the fully illuminated fiber and the partially illuminated fiber in Region 1, and the un-illuminated fiber in Region 2.

310 nm where a fully illuminated fiber can clearly be seen along with the presence of a partially illuminated fiber in Region 1. The light dispersion is summed between the bounds, illustrated in Figure 3b by the vertical dashed lines, to obtain the total signal for a given wavelength. We apply the standard nadir calibration described in Willame et al. (2022) to perform a spectral calibration of the Phobos and Deimos observations. Since the standard radiometric calibration requires 19 illuminated optical fibers, radiometric calibration would require an accurate estimation of the fraction to which the fibers are illuminated, which is planned but outside the scope of the present paper. In this first analysis, we normalize the spectra to 535 nm to study the spectral slope of the Phobos and Deimos spectra and permit direct comparison of the reflectance with previously published observations.

The Deimos observations are processed in the same way as Phobos, with the exception that for Deimos only a single fiber is illuminated (same fiber as the brightest Phobos fiber in Figure 3). To improve the SNR of the Deimos observation, we combined all frames that had a SNR > 50% of the peak value and bin resultant combined frames into spectral bins with a width of 10 nm. While spectral binning lowers the spectral resolution, it increases the SNR by a factor of ~2.5.

## 4. Results and Discussion

### 4.1. Comparison to Previous Phobos Observations

The surface reflectance spectrum of Phobos between 250 and 650 nm obtained by UVIS is shown in Figure 4a and compared to previous observations by the ultraviolet spectrometer (UVS) on Mariner 9 (Pang et al., 1978), the combined KRFM and ISM spectra aboard Phobos 2 (Murchie et al., 1991), HST FOS (Zellner & Wells, 1994), the IMP on Pathfinder (Murchie et al., 1999), OMEGA aboard Mars Express, CRISM on the Mars Reconnaissance Orbiter (Fraeman et al., 2012) and OSIRIS NAC-WAC aboard Rosetta (Pajola et al., 2013); see Table 1.

As done in Pajola et al. (2012), all spectra have been normalized to 535 nm to enable a direct comparison of spectral shape between the different instruments. The gap in the UVIS data between 390 and 410 nm is associated with the dichotomy in the second-order filter that causes an artifact in all UVIS spectra (Patel et al., 2017).
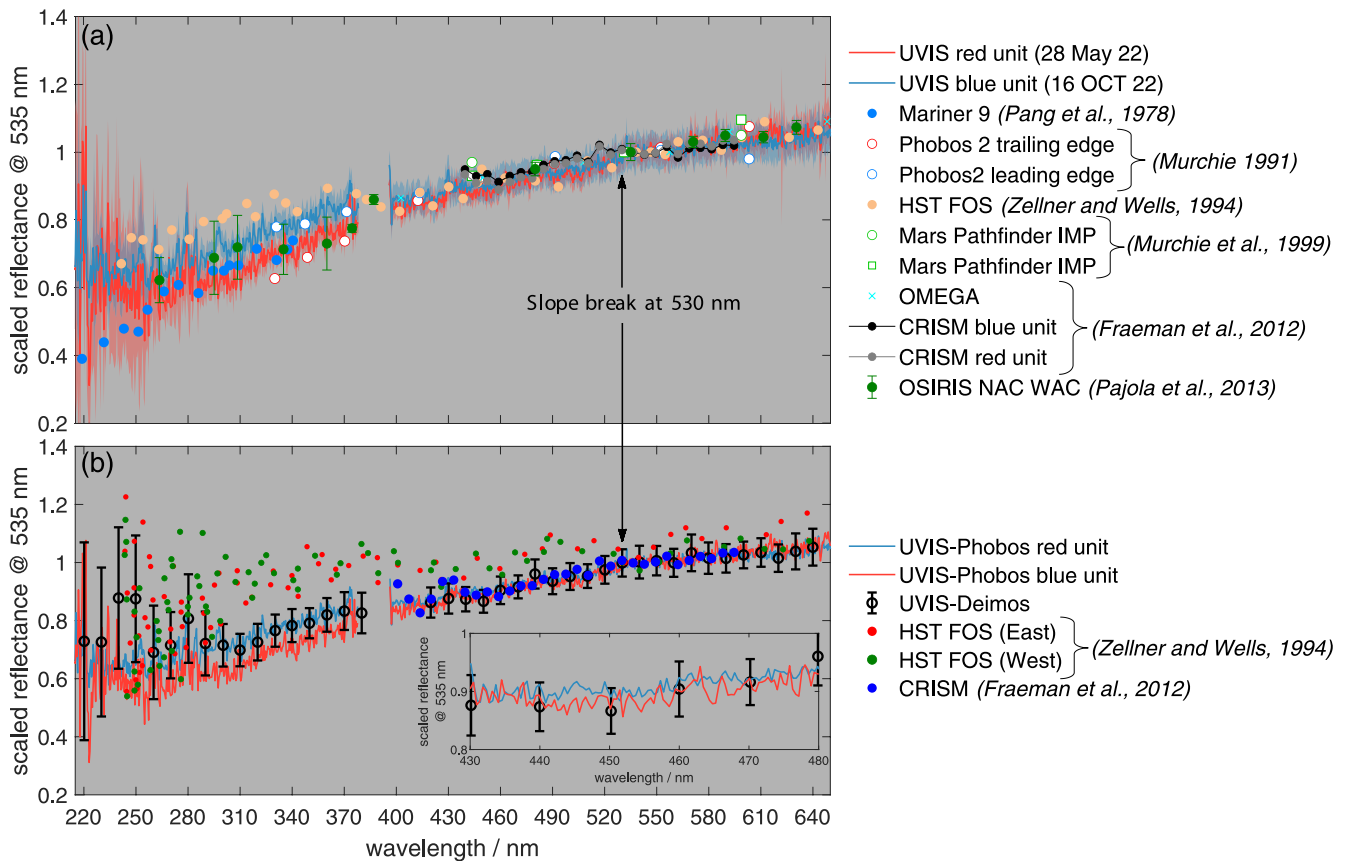
**Figure 4.** (a) Comparison of the UVIS Phobos blue unit spectrum (blue line) and red unit spectrum (red line) against those made by other instruments. The blue and red shading gives the uncertainty in the UVIS data. Also shown are the Phobos spectra measured by Mariner 9 (light blue circles), Phobos 2 leading (blue-white circles) and trailing (red-white circles) edge of Phobos, HST FOS (orange circles), IMP (green-white circles and squares), OMEGA (red crosses), the CRISM blue unit (black circles) and red unit (gray circle) and OSIRIS (dark green circles). (b) The UVIS Deimos spectra (black line) compared to other Deimos spectra measured by the, Hubble Space Telescope (HST) Faint Object Spectrograph (FOS) red and green dots and the Compact Reconnaissance Imaging Spectrometer for Mars (CRISM) (blue dots). We also show the two UVIS Phobos spectra (blue and red lines) for comparison. The inset in (b) shows a zoomed in the region around potential broad absorption centered near 0.45 µm.

The UVIS Phobos spectrum shows a characteristic red-slope, generally smooth trend, and not characterized by significant absorption features. There may be a slight flattening of the spectrum at wavelengths >530 nm relative to the near ultraviolet, which could be the edge of the 0.65 µm absorption feature (Binzel et al., 2001, 2004; Fraeman et al., 2014; Murchie et al., 1999). The UVIS observation May-22 shows a slightly steeper red slope compared to Oct-22 at visible wavelengths and exhibits a noticeably steeper UV drop-off at wavelengths shorter than 400 nm. The difference between the two UVIS observations is attributed to the fact that they observed different proportions of the Phobos blue unit and red unit, with May-22 measuring the area south east of Stickney crater, which is dominated by the red unit (Murchie & Erard, 1996; Murchie et al., 1999), while Oct-22 observed further west covering a significant portion of Stickney crater and thus measuring a good portion of the blue unit.

Generally, good agreement is seen between UVIS and previous observations at wavelengths longer than 400 nm. At wavelengths shorter than 400 nm, observation May-22, which we attribute to the Phobos red unit, agrees well with the Mariner 9 observation and is also within the uncertainty of the OSIRIS measurements, both of which observed the trailing edge of Phobos which has been shown to be dominated by the Phobos red unit (Murchie & Erard, 1996). Nevertheless, the UVIS spectrum is brighter than the Phobos trailing hemisphere measurements by Phobos 2 which perhaps suggests some portion of the blue unit was observed.

By comparison, observation Oct-22 shows a shallower UV drop-off and agrees more closely with measurements using Phobos 2 and HST FOS, both of which measured the Phobos leading hemisphere, which is dominated by the Phobos blue unit. Compared to Oct-22, the HST FOS spectrum is brighter at shorter wavelengths with a

**Table 1**
*Characteristics of Observations of Phobos and Deimos at UV and Visible Wavelengths*

| Instrument/Spacecraft | Wavelength range (μm) | Spectral resolution | Detected absorption bands (μm) | Reference | Notes |
|---|---|---|---|---|---|
| Mariner 9 ultraviolet spectrometer | 0.21–0.35 | 1.5 nm | | Pang et al. (1978) | Phobos—red unit |
| Viking lander camera | 0.4–1.1 | Narrow band filters with half widths of 100 nm | | Pang et al. (1978) | The Viking lander took disc integrated images of the sub-Mars hemisphere |
| Ground-based photometry | 0.5–1.0 | $\lambda/\Delta\lambda \sim 100$ | 0.65 | Pang et al. (1978) | Phobos red and blue unit |
| Phobos 2: KRFM | 0.32–0.6 | $\lambda/\Delta\lambda \sim 10$ | 0.65 μm | Murchie and Erard (1996) | Phobos red and blue unit |
| Phobos 2: ISM | 0.76–3.16 | $\lambda/\Delta\lambda \sim 50$ | | Murchie and Erard (1996) | |
| HST: FOS | 0.21–0.8 | 0.3 nm (210 nm) 20 nm (800 nm) | | Zellner and Wells (1994) | Observed both Phobos blue unit and Deimos |
| Pathfinder: IMP | 0.44–1.1 | Variable width filters with Bandwidths range from 18.9 to 40.8 nm | 0.65 | Murchie et al. (1999) | IMP measured the sub-Mars hemisphere of Phobos which is believed to contain both the red and blue geological units. |
| Mars Express: OMEGA | 0.35–5.0 | 7.0 nm (0.35–1.105 μm) | | Fraeman et al. (2012) | Observations of the Phobos red and blue unit |
| MRO: CRISM | 0.4–3.9 | ~6.55 nm | 0.65 2.8 | Fraeman et al. (2012) | Observations of the Phobos red and blue unit as well as Deimos |
| Rosetta: OSIRIS NAC-WAC | 0.26–0.99 | Variable width filters, FWHM of the filters ranged from 21 to 83 nm | 0.6 | Pajola et al. (2013) | Measured the Phobos red unit |

flatter gradient across the UV. Given the size of the UVIS footprint on the Phobos surface, we suspect that observation Oct-22, while observing predominately the blue unit, still observed a mix of both spectral units. This could likely explain the steeper UV gradient compared to HST FOS.

Reflectance data on Deimos are more sparse, but in Figure 4b we show a comparison of the UVIS Deimos spectrum (binned to a resolution of 10 nm to improve the SNR) to the spectra measured by the HST FOS (Zellner & Wells, 1994) and CRISM (Fraeman et al., 2012). The Deimos spectrum is generally consistent within measurement uncertainties with that of the Phobos red unit, with a red-sloped spectrum and no distinct spectral features. When compared to previous observations, the UVIS Deimos measurement does not generally agree with the FOS measurements, with the UVIS spectrum showing a steeper red-sloped gradient and a greater UV drop-off. Somewhat closer agreement is seen at shorter wavelengths (<300 nm); however, this could be due to the higher scatter in the FOS data and the larger uncertainties in the UVIS data at these wavelengths. The UVIS and CRISM spectra show better agreement with a similar red slope across visible wavelengths.

### 4.2. Possible Spectral Features for Insights Into Minerology

In the wavelength range of the NOMAD UVIS spectrometer (0.2–0.65 μm), a number of absorption features may be present and have been variously identified by different investigators. We examine these detections in light of our new UVIS data and include a discussion of potentially new absorption features. It should be noted that these putative absorption bands are weak, and their detection or non-detection would be a function of the portion of the moon imaged, signal to noise ratio, wavelength range, and spectral resolution. No specific absorption band has been detected in all data sets where common wavelength coverage exists.

#### 4.2.1. Spectral Features Between 0.4 and 0.465 μm

HST FOS spectra (Zellner & Wells, 1994) show a possible absorption band centered near 0.40 μm, a ~0.4 μm region absorption band. According to Zellner and Wells (1994), a similar feature is seen in a number of metamorphic carbon-dominated materials that are also dark, red-sloped, and otherwise spectrally featureless. If

present, such a band could be indicative of the presence of organic materials, specifically aromatic carbon π-π* transitions, seen commonly in metalloporphyrins, and termed the Soret band (e.g., Dunning & Moore, 1957; Gouterman, 1978). Absorption bands are seen in a variety of porphyrin-bearing geological materials such as oil shales (Holden & Gaffey, 1990), as well as in a reflectance spectrum of the CI1 CC Orgueil (Holden & Gaffey, 1987), and possibly in reflectance spectra of asteroid (2) Pallas (Vilas et al., 1993). Porphyrins are present in Orgueil (Hodgson & Baker, 1964). Unfortunately, this wavelength region is close to the second order filter dichotomy and thus not well sampled by UVIS. MAVEN/IUVS observations of the trailing hemisphere of Phobos showed "marginal evidence for an absorption feature longward of 300 nm, potentially produced by organic compounds" (Chaffin et al., 2017).

The UVIS spectra show a potential broad feature centered near 0.45–0.46 μm consistent with a spin-forbidden band associated with $Fe^{3+}$ in tetrahedral coordination in minerals such as serpentinites (Greenberger et al., 2015) and ferric iron sulfates (Cloutis et al., 2006). The 0.45 μm feature is more prominent in May-22, and Deimos observation compared to Oct-22, which observed more of the Phobos blue unit compared to May-22. The red unit and Deimos spectra exhibiting stronger absorption bands are consistent with other spectral features, namely the 0.65 and 2.8 μm bands, which have been shown to be either weaker or, in the case of the 0.65 μm band, absent in the blue unit (Fraeman et al., 2014).

### 4.2.2. Spectral Features Between 0.5 and 0.65 μm

A weak slope break and/or "shelf" in the 0.5–0.6 μm region is seen in the UVIS spectra where the spectral gradient changes to a shallower slope relative to shorter wavelengths (see Figure 4). Fraeman et al. (2012) presented OMEGA spectra of global Phobos, which show a change in slope and a region of constant reflectance (shelf) between ~0.5 and 0.6 μm; similarly, CRISM spectra of Phobos and Deimos show a similar feature (Fraeman et al., 2014), but it was not discussed. A slope break near 0.5 μm is seen in some spectra of the CI1 CC Orgueil (Cloutis et al., 2011), but its cause is uncertain. Some magnetite reflectance spectra do show a flat spectral slope or shallow absorption band in the 0.5–0.6 μm interval (Izawa et al., 2019), but also show other features not consistent with the martian moon spectra, such as a broad 1 μm region absorption feature. A 0.5–0.6 μm feature is seen in some plagioclase feldspar spectra, and a slope break is seen in many lunar regolith samples. This feature is likely attributable to $Fe^{2+}$-associated absorption.

The flattening of the spectrum could also be associated with the broad shallow absorption feature centered near 0.65 μm identified in multiple observational data of the martian moons (Fraeman et al., 2014; Murchie & Erard, 1996; Murchie et al., 2008; Pajola et al., 2013). Its depth ranges from ~0.5% to 5%, and its presence and strength is correlated with the slope of the visible to near infrared spectral continuum, specifically: $R_{average(0.40-0.50)}/R_{average(0.75-0.85)}$ (Fraeman et al., 2014), with the Phobos red unit displaying a higher band depth. Following Fraeman et al. (2014), we attempted to determine whether the observed slope break observed in the UVIS data is associated with the 0.65 μm absorption by subtracting a linear continuum between 0.5 and 0.85 μm from the UVIS Phobos and Deimos spectra. While UVIS does not measure the longer wavelengths required for such an analysis, fortuitously the observing geometry of the CRISM (FRT00002992_03) and UVIS observations are similar, with both viewing the sub-Mars hemisphere, as illustrated in Figures 1a, 1b, and 5a. The similarity in the view geometry allowed us to project the UVIS FOV onto the CRISM image and, by averaging all the CRISM pixels that were within the UVIS FOV, to derive an equivalent CRISM spectra for the UVIS observations of Phobos, thus providing an extended wavelength range. The derived CRISM spectra for the UVIS observations, May-22 (MAY-22[CRISM]) and Oct-22 (OCT-22[CRISM]) are shown in Figure 5b. Not unexpectedly, the MAY-22[CRISM] spectrum is very similar to the Phobos red unit spectrum derived by Fraeman et al. (2014) given that the location of the UVIS footprint for the May-22 observation is over an area suspected to be dominated by the red unit. While the Oct-22 observation measured a portion of the Stickney crater and the Phobos blue unit, the Oct-22[CRISM] spectrum displays a noticeably steeper gradient across NIR wavelengths compared to the CRISM blue unit. This spectrum has a slope that, while shallower than the CRISM red unit, still sits more closely to the Phobos red unit. This supports the observational evidence that the Oct-22 spectrum is a composite of both geological units given the relatively large footprint of UVIS. A linear continuum between 0.5 and 0.85 μm was calculated from the derived CRISM spectra and subtracted from both the CRISM and UVIS spectra for May-22 and Oct-22 (binned to a 10 nm resolution to improve the SNR close to the detector edge). For comparison we also subtract a linear continuum from the UVIS Deimos spectrum (calculated from the CRISM Deimos spectrum) and the OSIRIS Phobos data and show their resultant continuum removed spectrum alongside those for May-22 and Oct-22 in
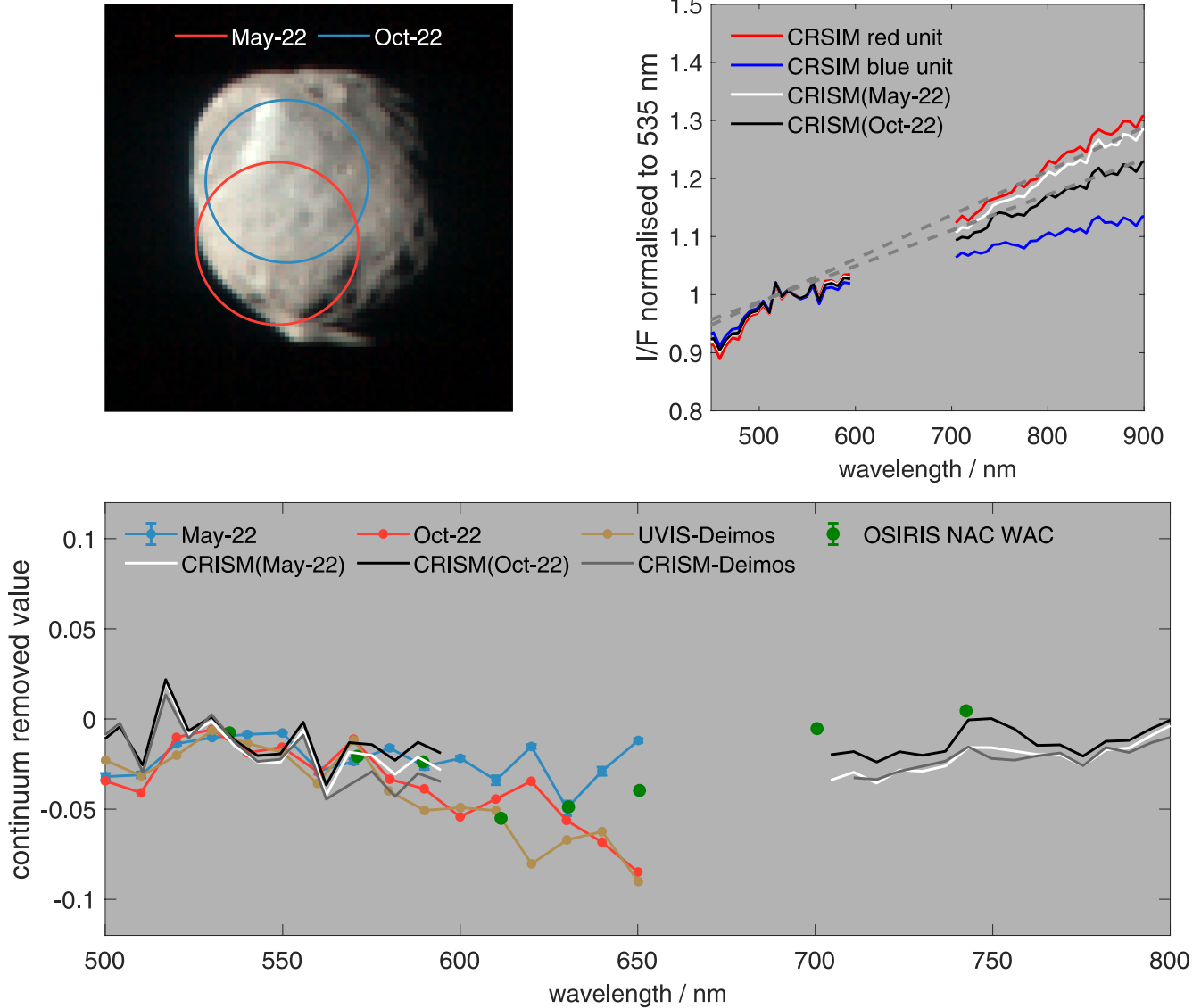
**Figure 5.** (a) Illustration of the UVIS FoV projected onto the CRISM Phobos observation (FRT00002992_03) for May-22 (red circle) and Oct-22 (blue circle). (b) The reflectance spectrum normalized to 535 nm derived from CRSIM data for UVIS observations May-22 (white line) and Oct-22 (black line) and the Phobos red unit (red line) and blue unit (blue line) as measured by CRISM (Fraeman et al., 2014). (c) Shows the continuum removed spectrum for the UVIS observations, May-22 (red line), Oct-22 (blue line), and Deimos (brown line), OSIRIS (green circles) (Pajola et al., 2013), and the CRISM-derived spectra for May-22 (while line) and Oct-22 (black line).

Figure 5c. The continuum removed spectra of UVIS are similar to those derived from CRISM and OSIRIS, displaying a shallow, negative spectral gradient from 0.53 to 0.61 μm, consistent with the 0.65 μm absorption feature. As expected, the May-22 and Deimos spectra show a similar spectral slope and potential band depth, consistent with May-22 measuring the Phobos red unit. Oct-22 exhibits a shallower gradient toward 0.65 μm compared to both the May-22 and Deimos spectra. This provides further observational evidence that the Oct-22 spectrum contains some portion of the Phobos blue unit, which was shown by Fraeman et al. (2014) not to exhibit the 0.65 μm absorption feature. Our analysis suggests that the likely cause of the slope break near 0.53 μm in the UVIS Phobos and Deimos spectra is a result of the previously identified 0.65 μm absorption feature.

A similar absorption feature has also been observed in the red-sloped spectra of low albedo asteroids but as noted by Fraeman et al. (2014), multiple absorption processes can result in a spectral feature near 0.65 μm, including $Fe^{2+}$ and $Fe^{3+}$ electronic transitions, $Fe^{2+}$–$Fe^{3+}$ charge transfers, and metallic iron absorptions combined with
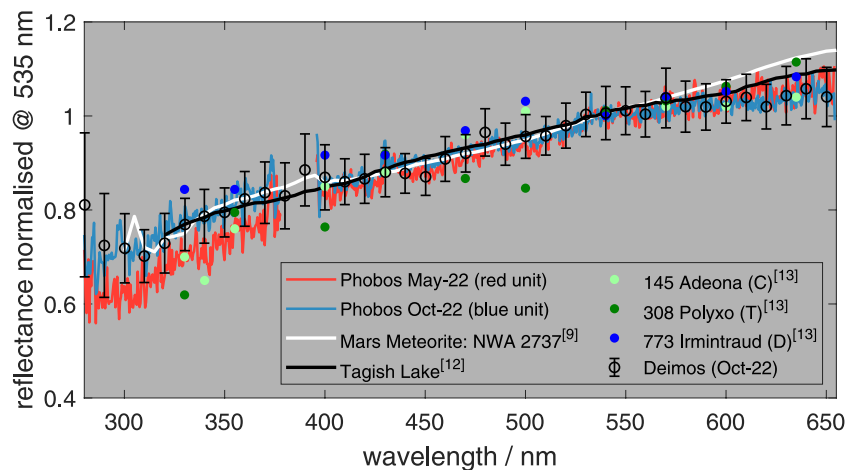
**Figure 6.** The observed reflectance spectrum of the Deimos (open black circles), Phobos blue unit (blue line) and Phobos red unit (red line) compared against the spectra of known asteroids, 145 Adeona (C-type) (orange dots), 308 Polyxo (T-type) (green dots), 773 Irmintraud (D-type) (blue dots) and also the Tagish lake (black line) and Mars meteorite NWA 2737 (white line) samples. Observations are normalized to 535 nm to compare the spectral shape.

Rayleigh scattering by nanophase particles (Clark et al., 2012; Morris et al., 1985). The assignment of this (single) feature to a unique mechanism or specific phase is difficult (King & Clark, 1997).

Mineralogically, this feature can be plausibly attributed to desiccated Fe-phyllosilicates or space weathered exogenic materials, producing Fe and OH. In the case of phyllosilicates, a band centered near 0.65 µm is most consistent with saponitic and/or serpentinitic phyllosilicates and is attributable to $Fe^{3+}$–$Fe^{2+}$ charge transfers; it can be seen in reflectance spectra of CCs that are otherwise largely featureless (Cloutis et al., 2011).

Attributing this feature to heated phyllosilicates would be consistent with phyllosilicate-rich ejecta from Mars, as naturally heated CCs do not show the red-sloped spectra of the martian moons (Cloutis, Hudon, Hiroi, & Gaffey, 2012). Attributing this feature to metallic iron would be consistent with space weathering of Fe-bearing materials, which could derive from basaltic or carbonaceous chondrite targets. Its correlation with spectral slopes would also be consistent with space weathering as this absorption feature is absent in the presumably less space weathered Phobos blue unit associated with Stickney crater. An alternative explanation for this feature is its association with olivine (Gaffey, 1998; King & Ridely, 1987). However, it is generally weak, and if associated with $Fe^{2+}$, would be expected to be accompanied by stronger $Fe^{2+}$-associated absorption bands in the 0.9–1.3 µm region.

### 4.3. Discussion

The lack of definitive absorption bands at UV-visible wavelengths, and being reliant on albedo and spectral slope alone, limits our ability to elucidate the composition of Phobos and Deimos. However, we can provide inferences about the composition and origin of the moons through spectral comparisons with other known airless bodies and meteorites. In Figure 6, we present a comparison of the UVIS Phobos "red unit" May-22 spectrum and the UVIS Phobos "blue unit" spectrum Oct-22 against the spectra of known C-type (145 Adeona), D-type (773 Irmintraud) and T-type (308 Polyxo) asteroids (Chapman et al., 2005) to make a possible taxonomical comparison with Phobos. We also show a comparison with the Tagish Lake meteorite sample (Hiroi et al., 2001), which is considered as a possible Phobos-like analog meteorite (Fraeman et al., 2012; Pajola et al., 2012), and the Mars meteorite NWA 2737 sample. NWA 2737 is a dunite with a composition that is 87% olivine, but it is unusually dark brown in color likely associated with its high shock level (Pieters et al., 2008; Treiman et al., 2007). Unlike more common terrestrial olivines, the NWA 2737 UV and visible spectrum has a low albedo and a strong red-slope with weak ferrous absorptions in the 1 µm region (Pieters et al., 2008). Figure 6 provides a spectral comparison of the UVIS Deimos spectrum to the same asteroids and meteorite samples.

The UVIS measurements confirm previous studies (Fraeman et al., 2012, 2014; Murchie & Erard, 1996; Pajola et al., 2013, 2018) that suggest, at least spectrally, that Phobos and Deimos are more akin to T- and D-type

asteroids than to C-type asteroids, with a distinctly redder slope across visible wavelengths. The Phobos red unit and Deimos spectra tend toward greater likeness to the redder sloped T-type asteroid and also the Tagish Lake meteorite, which itself is thought to be analogous to T-type asteroids (Hiroi et al., 2001; Pajola et al., 2013, 2018). On the other hand, the blue unit appears to be spectrally closer to the D-type asteroid, a shallower gradient at longer wavelengths and a reduced UV drop-off. The spectral similarity to D-type and T-type asteroids alone cannot confirm Phobos and Deimos as being captured asteroids however, since as discussed by Hyodo, Genda, et al. (2017) and Hyodo, Rosenblatt et al. (2017), the spectral similarity to primitive D-type and T-type asteroids could be explained by the moons having formed at the outer reaches of an accretion disk after a giant collision which later migrated inward. The accreted material would, according to Hyodo, Genda, et al. (2017) and Hyodo, Rosenblatt et al. (2017), consist of a mixture of melted and highly shocked martian and impactor materials. This leaves open the possibility of a wide range of lithologies.

The Tagish Lake C2 ungrouped chondrite is generally spectrally featureless and shows good spectral likeness to Phobos and Deimos across the UVIS wavelength range, as previously reported by Fraeman et al. (2014) and Pajola et al. (2013). Different lithologies have variable spectral slopes ranging as high as Phobos red material (Cloutis, Hudon, Hiroi, Gaffey, Mann, 2012; Izawa et al., 2015). Pajola et al. (2013) found that a modeled mixture of the Tagish Lake CC plus a spectrally nearly-featureless basaltic glass powder matched both the albedo and spectral slope of the Phobos red unit from 0.3 to ~3.5 μm. In the ultraviolet spectrum, various lithologies of Tagish Lake show weak absorption features near 0.22 and 0.27 μm that are attributable to $Fe^{3+}$-O and $Fe^{2+}$-O charge transfers, respectively (Izawa et al., 2015). The weak signal at short wavelengths in the UVIS data prevents confirmation of whether similar absorptions are present in the Phobos and Deimos spectra.

Reflectance spectra of the Mars meteorite NWA 2737 show some spectra with a red-sloped continuum similar to red material at wavelengths <550 nm. Analysis of the brown olivine in NWA 2737 by Pieters et al. (2008) concluded that the most likely cause of the red-sloped continuum and suppressed ferrous absorption was the presence of shock-induced nanophase metallic iron particles ($npFe^0$) finely dispersed throughout the brown olivine. However, the reflectance spectrum of this meteorite shows a ubiquitous $Fe^{2+}$-associated absorption band in the 1 μm region, unlike Phobos. This feature appears to be highly persistent in the face of space weathering and melting (e.g., Battler & Spray, 2009; Loeffler et al., 2009; Yamada et al., 1999). Noble et al. (2007) demonstrated that even small amounts of $npFe^0$ embedded in silicate can have a significant effect on the visible and near-IR spectrum of the host material, producing a darker red-sloped spectrum with significantly suppressed mineral absorption bands, similar to what we see for the martian moons. This leads to the enticing question on the potential role embedded $npFe^0$ could have in explaining the observed red-sloped and near featureless spectrum of Phobos and Deimos. Spectroscopic studies (Cloutis et al., 1990a, 1990b, 1990c, 2009; Singer, 1981) involving olivine mixed with various opaque materials, such as metallic iron, graphite, and iron oxides, can diminish spectral bands across UV to NIR wavelengths, which could partially explain the lack of $Fe^{2+}$ electronic absorptions, diagnostic of olivine and pyroxene in the CRISM data (Fraeman et al., 2014).

Determining the composition of Phobos (and Deimos), as either captured asteroids or re-accreted ejecta from a giant impact on Mars, is not straightforward as their surface may consist of a mixture of martian, martian impactor, and asteroidal/zodiacal dust (e.g., Fries et al., 2017). The giant impact hypothesis suggests that the composition of Phobos may be ~50/50 Mars/impactor, with, as mentioned, the composition of the impactor being essentially unknown (Hyodo, Genda, et al., 2017). The ejecta would be mostly molten with a small amount of vapor (Hyodo, Genda, et al., 2017). It is expected that a giant-impact origin of the martian moons may be dominated by vaporized material (Craddock, 2011), although the existence of low shock-level martian meteorites suggests that unshocked or unmelted materials could be ejected from the surface of Mars and reaccreted.

After their formation or capture, subsequent impacts on Mars can insert ejecta into Phobos-crossing orbits (e.g., Patel et al., 2019), and Phobos will also encounter solar system projectiles. Modeling suggests that the two processes add, at most, 3% material to the regolith of Phobos, with the bulk coming from solar system projectiles (Ramsley & Head, 2013). In addition to projectiles, dust may be deposited on their surfaces at a rate of <14–26 μm/year (Miyamoto et al., 2021), and over 4 Ga could accumulate a ~200–300 cm thick surface layer (Fries et al., 2017). Mass transfer between Phobos and Deimos is also probable based on geomorphological observations and impact modeling (Nayak et al., 2016). Finally, space weathering, whose spectrum-altering properties are not well constrained, could change the spectroscopic properties of the moons' surfaces (e.g., Pieters et al., 2014).

The spectral differences between the Phobos red unit and Deimos as compared to the Phobos blue unit, which is largely associated with Stickney crater on Phobos, may be attributable to space weathering, where Stickney crater represents younger material (Ramsley & Head, 2017). However, stratigraphic relationships and areal distribution suggest that the red unit may not simply derive from space weathering of the blue unit (Pieters et al., 2014). A similar analysis of observational data for the dark near-Earth asteroids Bennu and Ryugu also suggests that space weathering trends on dark asteroids are complex (Clark et al., 2023).

## 5. Conclusions

The spectral reflectance of Phobos and Deimos has the potential to provide constraints on the composition of Phobos and Deimos and ultimately elucidate the origin of these two moons. In this study, we present the reflectance of Phobos and Deimos at ultraviolet and visible wavelengths measured by NOMAD-UVIS onboard TGO. Comparisons of these measurements with previous observations by other instruments have proved to be in good agreement, showing a relatively featureless and predominately red-sloped spectrum similar to D-type and T-type asteroids.

The UVIS data alone are insufficient to determine the composition of Phobos and Deimos. The future Martian Moons eXploration (MMX) mission (Kuramoto et al., 2022) will perform a comprehensive analysis of the martian moons through a combination of visible-infrared, Gamma-ray & Neutron, and ion-mass spectroscopy observations in order to determine the elemental composition of the moons. Further high-resolution UV-VIS observations by NOMAD in collaboration with MMX will allow us to further elucidate the origin of the moons of Mars.

## Appendix A: Comparison of All UVIS Phobos Spectra

For clarity, in the manuscript we restrict our analysis to two UVIS Phobos observations performed on May 28, 2022 and the 16 October 2022, for reasons of clarity. The observation characteristics meant that approximately the same general face of the Phobos surface was repeatedly observed. Hence, the Phobos spectra were all very similar and showing them all did not add to the discussion in the paper. We therefore restricted the discussion to focus on the two observations that represented the highest quality data and, more importantly, the mostly likely candidates for the two color units located on the surface of Phobos. The rest of the UVIS spectra sit somewhere between these two observations with a mixture of coverage of red/blue units in each observation as we show in Figure A1 by the black lines. Comparing all the observations, very little difference is seen in the UVIS spectra at visible wavelengths >420 nm. At shorter wavelengths each spectrum becomes slightly more distinct, either slightly bluer or redder depending on the proportion of the blue and red unit within the UVIS footprint during the observation. The two observations discussed in this paper are shown as the bold red (May-22) and bold blue (Oct-22) lines and bound to the other observations.
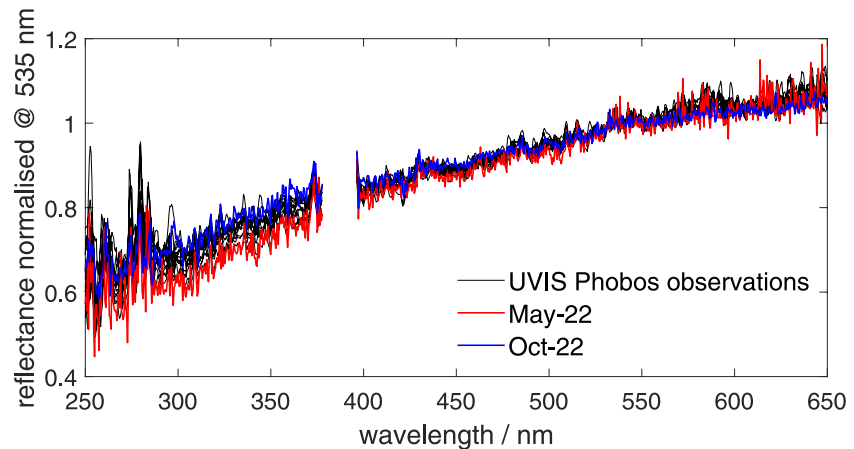
**Figure A1.** The reflectance spectrum of Phobos normalized to unity at 535 nm for all UVIS observations of Phobos. In the observations presented in this work, May-22 (red line) defines the "reddest" spectrum and Oct-22 (blue line) the "bluest" spectrum. The other Phobos spectra are shown in black and sit between May-22 and Oct-22. The inset zooms in the 300–370 nm region to more clearly show the spectral variation in the UVIS observations.

## Data Availability Statement

Public access to all ExoMars TGO data is available through the ESA Planetary Science Archive (archives.esac. esa.int/psa/). The Asteroid spectral data used in the comparisons were taken from Chapman et al. (2005) and the meteorite data from the RELAB Spectral Library (Milliken, 2020). The reflectance spectra of Phobos and Deimos from NOMAD-UVIS measurements used in this article are publicly available via the Open Research Data Online (ORDO) data repository (Mason & Patel, 2023).

## References

Acton, C., Bachman, N., Semenov, B., & Wright, E. (2018). A look towards the future in the handling of space science mission geometry. *Planetary and Space Science*, *150*, 9–12. https://doi.org/10.1016/j.pss.2017.02.013

Acton, C. H., Jr. (1996). Ancillary data services of NASA's navigation and ancillary information facility. *Planetary and Space Science*, *44*(1), 65–70. https://doi.org/10.1016/0032-0633(95)00107-7

Battler, M. M., & Spray, J. G. (2009). The Shawmere anorthosite and OB-1 as lunar highland regolith simulants. *Planetary and Space Science*, *57*(14–15), 2128–2131. https://doi.org/10.1016/j.pss.2009.09.003

Bell, J. F., Fanale, F., & Cruikshank, D. P. (1993). Chemical and physical properties of the Martian satellites. *Resources of Near-Earth Space*, 887–901.

Bibring, J. P., Soufflot, A., Berthé, M., Langevin, Y., Gondet, B., Drossart, P., et al. (2004). OMEGA: Observatoire pour la Minéralogie, l'Eau, les Glaces et l'Activité. In A. Wilson, & A. Chicarro (Eds.), *Mars Express: The scientific payload* (Vol. 1240, p. 37–49). ESA Publications Division.

Binzel, R. P., Harris, A. W., Bus, S. J., & Burbine, T. H. (2001). Spectral properties of near-Earth objects: Palomar and IRTF results for 48 objects including spacecraft targets (9969) Braille and (10302) 1989 ML. *Icarus*, *151*(2), 139–149. https://doi.org/10.1006/icar.2001.6613

Binzel, R. P., Rivkin, A. S., Stuart, J. S., Harris, A. W., Bus, S. J., & Burbine, T. H. (2004). Observed spectral properties of near-Earth objects: Results for population distribution, source regions, and space weathering processes. *Icarus*, *170*(2), 259–294. https://doi.org/10.1016/j.icarus.2004.04.004

Burns, J. A. (1978). The dynamical evolution and origin of the Martian moons. *Vistas in Astronomy*, *22*, 193–210. https://doi.org/10.1016/0083-6656(78)90015-6

Burns, J. A. (1992). Contradictory clues as to the origin of the Martian moons. *Mars*, 1283–1301. https://doi.org/10.2307/j.ctt207g59v.42

Chaffin, M., Deighan, J., Schneider, N. M., Thiemann, E., Stewart, I. F., Jain, S., et al. (2017). The UV spectrum of Phobos as measured by MAVEN/IUVS. In *AGU fall meeting abstracts* (Vol. 2017, p. P23F-01).

Chapman, C. R., Gaffey, M., & McFadden, L. (2005). 24-color asteroid survey. *NASA Planetary Data System, EAR-A.34.*

Chapman, C. R., McCord, T. B., & Johnson, T. V. (1973). Asteroid spectral reflectivities. *The Astronomical Journal*, *78*, 126–140. https://doi.org/10.1086/111388

Clark, B. E., Sen, A., Zou, X. D., Dellagiustina, D. N., Sugita, S., Sakatani, N., et al. (2023). Overview of the search for signs of space weathering on the low-albedo asteroid (101955) Bennu. *Icarus*, *115563*, 115563. https://doi.org/10.1016/j.icarus.2023.115563

Clark, R. N., Cruikshank, D. P., Jaumann, R., Brown, R. H., Stephan, K., Dalle Ore, C. M., et al. (2012). The surface composition of Iapetus: Mapping results from Cassini VIMS. *Icarus*, *218*(2), 831–860. https://doi.org/10.1016/j.icarus.2012.01.008

Cloutis, E. A. (1997). Manganese-rich olivines: Identification from spectral reflectance properties. *Journal of Geophysical Research*, *102*(E11), 25575–25580. https://doi.org/10.1029/97je02497

Cloutis, E. A. (2002). Pyroxene reflectance spectra: Minor absorption bands and effects of elemental substitutions. *Journal of Geophysical Research*, *107*(E6), 6-1–6.12. https://doi.org/10.1029/2001je001590

Cloutis, E. A., Gaffey, M. J., Smith, D. G., & Lambert, R. S. J. (1990a). Metal silicate mixtures: Spectral properties and applications to asteroid taxonomy. *Journal of Geophysical Research*, *95*(B6), 8323–8338. https://doi.org/10.1029/JB095iB06p08323

Cloutis, E. A., Gaffey, M. J., Smith, D. G., & Lambert, R. S. J. (1990b). Reflectance spectra of "featureless" materials and the surface mineralogies of M-and E-class asteroids. *Journal of Geophysical Research*, *95*(B1), 281–293. https://doi.org/10.1029/JB095iB01p00281

Cloutis, E. A., Gaffey, M. J., Smith, D. G., & Lambert, R. S. J. (1990c). Reflectance spectra of mafic silicate-opaque assemblages with applications to meteorite spectra. *Icarus*, *84*(2), 315–333. https://doi.org/10.1016/0019-1035(90)90041-7

Cloutis, E. A., Hardersen, P. S., Reddy, V., Gaffey, M. J., Bailey, D. T., & Craig, M. A. (2009). Metal-Orthopyroxene and Metal-Olivine Mixtures: Spectral reflectance properties and implications for asteroid spectroscopy. In *40th annual lunar and planetary science conference* (p. 1332). https://doi.org/10.1016/j.icarus.2010.12.009

Cloutis, E. A., Hawthorne, F. C., Mertzman, S. A., Krenn, K., Craig, M. A., Marcino, D., et al. (2006). Detection and discrimination of sulfate minerals using reflectance spectroscopy. *Icarus*, *184*(1), 121–157. https://doi.org/10.1016/j.icarus.2006.04.003

Cloutis, E. A., Hiroi, T., Gaffey, M. J., Alexander, C. O. D., & Mann, P. (2011). Spectral reflectance properties of carbonaceous chondrites: 1. CI chondrites. *Icarus*, *212*(1), 180–209. https://doi.org/10.1016/j.icarus.2010.12.009

Cloutis, E. A., Hudon, P., Hiroi, T., & Gaffey, M. J. (2012). Spectral reflectance properties of carbonaceous chondrites 4: Aqueously altered and thermally metamorphosed meteorites. *Icarus*, *220*(2), 586–617. https://doi.org/10.1016/j.icarus.2012.05.018

Cloutis, E. A., Hudon, P., Hiroi, T., Gaffey, M. J., & Mann, P. (2012). Spectral reflectance properties of carbonaceous chondrites: 8."Other" carbonaceous chondrites: CH, ungrouped, polymict, xenolithic inclusions, and R chondrites. *Icarus*, *221*(2), 984–1001. https://doi.org/10.1016/j.icarus.2012.10.008

Craddock, R. A. (1994). The origin of Phobos and Deimos. In *Lunar and planetary science conference* (Vol. 25, p. 293).

Craddock, R. A. (2011). Are Phobos and Deimos the result of a giant impact? *Icarus*, *211*(2), 1150–1161. https://doi.org/10.1016/j.icarus.2010.10.023

Dunning, H. N., & Moore, J. W. (1957). Porphyrin research and origin of petroleum. *AAPG Bulletin*, *41*(11), 2403–2412. https://doi.org/10.1306/0BDA599F-16BD-11D7-8645000102C1865D

Fraeman, A. A., Arvidson, R. E., Murchie, S. L., Rivkin, A., Bibring, J. P., Choo, T. H., et al. (2012). Analysis of disk-resolved OMEGA and CRISM spectral observations of Phobos and Deimos. *Journal of Geophysical Research*, *117*(E11), E00J15. https://doi.org/10.1029/2012JE004137

Fraeman, A. A., Murchie, S. L., Arvidson, R. E., Clark, R. N., Morris, R. V., Rivkin, A. S., & Vilas, F. (2014). Spectral absorptions on Phobos and Deimos in the visible/near infrared wavelengths and their compositional constraints. *Icarus*, *229*, 196–205. https://doi.org/10.1016/j.icarus.2013.11.021

Fries, M., Cintala, M., Steele, A., & Welzenbach, L. C. (2017). Dust infall onto Phobos and Deimos can explain their carbonaceous reflectance signature, perhaps overlying a Mars-impact-origin core: A hypothesis. In *Lunar and planetary science conference (No. JSC-CN-38696)*.

Gaffey, M. J. (1998). Using nickel features in the spectra of olivine-dominated A-and S (I)-type asteroids to determine the oxidation state of the solar nebula. In *Lunar and planetary science conference* (Vol. 1370, p. 1370).

Gouterman, M. (1978). Optical spectra and electronic structure of porphyrins and related rings. *The Porphyrins*, *3*, 1–165. https://doi.org/10.1016/b978-0-12-220103-5.50008-8

Greenberger, R. N., Mustard, J. F., Cloutis, E. A., Pratt, L. M., Sauer, P. E., Mann, P., et al. (2015). Serpentinization, iron oxidation, and aqueous conditions in an ophiolite: Implications for hydrogen production and habitability on Mars. *Earth and Planetary Science Letters*, *416*, 21–34. https://doi.org/10.1016/j.epsl.2015.02.002

Hesselbrock, A. J., & Minton, D. A. (2017). An ongoing satellite–ring cycle of Mars and the origins of Phobos and Deimos. *Nature Geoscience*, *10*(4), 266–269. https://doi.org/10.1038/ngeo2916

Hiroi, T., Zolensky, M. E., & Pieters, C. M. (2001). The Tagish Lake meteorite: A possible sample from a D-type asteroid. *Science*, *293*(5538), 2234–2236. https://doi.org/10.1126/science.1063734

Hodgson, G. W., & Baker, B. L. (1964). Evidence for porphyrins in the Orgueil meteorite. *Nature*, *202*(4928), 125–131. https://doi.org/10.1038/202125a0

Holden, P. N., & Gaffey, M. J. (1987). The detection of porphyrin-like features in reflectance spectra of carbonaceous chondrites. *Meteoritics*, *22*, 412.

Holden, P. N., & Gaffey, M. J. (1990). Practical considerations for using reflectance spectroscopy as a screening tool for geoporphyrins. *Energy & Fuels*, *4*(6), 705–709. https://doi.org/10.1021/ef00024a015

Hyodo, R., & Charnoz, S. (2017). Dynamical evolution of the debris disk after a satellite catastrophic disruption around Saturn. *The Astronomical Journal*, *154*(1), 34. https://doi.org/10.3847/1538-3881/aa74c9

Hyodo, R., Genda, H., Charnoz, S., & Rosenblatt, P. (2017). On the impact origin of Phobos and Deimos. I. Thermodynamic and physical aspects. *The Astrophysical Journal*, *845*(2), 125. https://doi.org/10.3847/1538-4357/aa81c4

Hyodo, R., & Ohtsuki, K. (2015). Saturn's F ring and shepherd satellites a natural outcome of satellite system formation. *Nature Geoscience*, *8*(9), 686–689. https://doi.org/10.1038/ngeo2508

Hyodo, R., Rosenblatt, P., Genda, H., & Charnoz, S. (2017). On the impact origin of Phobos and Deimos. II. True polar wander and disk evolution. *The Astrophysical Journal*, *851*(2), 122. https://doi.org/10.3847/1538-4357/aa9984

Ida, S., Canup, R. M., & Stewart, G. R. (1997). Lunar accretion from an impact-generated disk. *Nature*, *389*(6649), 353–357. https://doi.org/10.1038/38669

Izawa, M. R., Cloutis, E. A., Rhind, T., Mertzman, S. A., Applin, D. M., Stromberg, J. M., & Sherman, D. M. (2019). Spectral reflectance properties of magnetites: Implications for remote sensing. *Icarus*, *319*, 525–539. https://doi.org/10.1016/j.icarus.2018.10.002

Izawa, M. R. M., Craig, M. A., Applin, D. M., Sanchez, J. A., Reddy, V., Le Corre, L., et al. (2015). Variability, absorption features, and parent body searches in "spectrally featureless" meteorite reflectance spectra: Case study–Tagish Lake. *Icarus*, *254*, 324–332. https://doi.org/10.1016/j.icarus.2015.04.013

Keller, H. U., Barbieri, C., Lamy, P., Rickman, H., Rodrigo, R., Wenzel, K. P., et al. (2007). OSIRIS–The scientific camera system onboard Rosetta. *Space Science Reviews*, *128*(1–4), 433–506. https://doi.org/10.1007/s11214-006-9128-4

King, T. V., & Clark, R. N. (1997). The presence of a single absorption feature: What it does and doesn't imply. In *Lunar and planetary science conference* (p. 727).

King, T. V., & Ridley, W. I. (1987). Relation of the spectroscopic reflectance of olivine to mineral chemistry and some remote sensing implications. *Journal of Geophysical Research*, *92*(B11), 11457–11469. https://doi.org/10.1029/JB092iB11p11457

Kuramoto, K., Kawakatsu, Y., Fujimoto, M., Araya, A., Barucci, M. A., Genda, H., et al. (2022). Martian moons exploration MMX: Sample return mission to Phobos elucidating formation processes of habitable planets. *Earth Planets and Space*, *74*(1), 1–31. https://doi.org/10.1186/s40623-021-01545-7

Loeffler, M. J., Dukes, C. A., & Baragiola, R. A. (2009). Irradiation of olivine by 4 keV He$^+$: Simulation of space weathering by the solar wind. *Journal of Geophysical Research*, *114*(E3), E03003. https://doi.org/10.1029/2008JE003249

Mason, J. P., & Patel, M. R. (2023). Radiance factor of Phobos and Deimos measured by UVIS [Dataset]. The Open University. https://doi.org/10.21954/ou.rd.23676801.v1

Mason, J. P., Patel, M. R., Leese, M. R., Hathi, B. G., Willame, Y., Thomas, I. R., et al. (2022). Removal of straylight from ExoMars NOMAD-UVIS observations. *Planetary and Space Science*, *218*, 105432. https://doi.org/10.1016/j.pss.2022.105432

Milliken, R. (2020). The RELAB spectral library bundle. The RELAB spectral library bundle contains reflectance spectra and ancillary data acquired at the Reflectance Experiment Laboratory (RELAB) at Brown University. https://doi.org/10.17189/1519032

Miyamoto, H., Niihara, T., Wada, K., Ogawa, K., Senshu, H., Michel, P., et al. (2021). Surface environment of Phobos and Phobos simulant UTPS. *Earth Planets and Space*, *73*(1), 1–17. https://doi.org/10.1186/s40623-021-01406-3

Morris, R. V., Lauer, H. V., Jr., Lawson, C. A., Gibson, E. K., Jr., Nace, G. A., & Stewart, C. (1985). Spectral and other physicochemical properties of submicron powders of hematite ($\alpha$-$Fe_2O_3$), maghemite ($\gamma$-$Fe_2O_3$), magnetite ($Fe_3O_4$), goethite ($\alpha$-FeOOH), and lepidocrocite ($\gamma$-FeOOH). *Journal of Geophysical Research*, *90*(B4), 3126–3144. https://doi.org/10.1029/JB090iB04p03126

Murchie, S., Arvidson, R., Bedini, P., Beisser, K., Bibring, J. P., Bishop, J., et al. (2007). Compact reconnaissance imaging spectrometer for Mars (CRISM) on Mars reconnaissance orbiter (MRO). *Journal of Geophysical Research*, *112*(E5), E05S03. https://doi.org/10.1029/2006JE002682

Murchie, S., & Erard, S. (1996). Spectral properties and heterogeneity of Phobos from measurements by Phobos 2. *Icarus*, *123*(1), 63–86. https://doi.org/10.1006/icar.1996.0142

Murchie, S., Thomas, N., Britt, D., Herkenhoff, K., & Bell, J. F., III. (1999). Mars pathfinder spectral measurements of Phobos and Deimos: Comparison with previous data. *Journal of Geophysical Research*, *104*(E4), 9069–9079. https://doi.org/10.1029/98JE02248

Murchie, S. L., Britt, D. T., Head, J. W., Pratt, S. F., Fisher, P. C., Zhukov, B. S., et al. (1991). Color heterogeneity of the surface of Phobos: Relationships to geologic features and comparison to meteorite analogs. *Journal of Geophysical Research*, *96*(B4), 5925–5945. https://doi.org/10.1029/90jb02354

Murchie, S. L., Choo, T., Humm, D., Rivkin, A. S., Bibring, J. P., Langevin, Y., et al. (2008). MRO/CRISM observations of Phobos and Deimos. In *39th annual lunar and planetary science conference* (Vol. 1391, p. 1434).

Nayak, M., Nimmo, F., & Udrea, B. (2016). Effects of mass transfer between Martian satellites on surface geology. *Icarus*, *267*, 220–231. https://doi.org/10.1016/j.icarus.2015.12.026

Noble, S. K., Pieters, C. M., & Keller, L. P. (2007). An experimental approach to understanding the optical effects of space weathering. *Icarus*, *192*(2), 629–642. https://doi.org/10.1016/j.icarus.2007.07.021

Pajola, M., Lazzarin, M., Bertini, I., Marzari, F., Turrini, D., Magrin, S., et al. (2012). Spectrophotometric investigation of Phobos with the Rosetta OSIRIS-NAC camera and implications for its collisional capture. *Monthly Notices of the Royal Astronomical Society*, *427*(4), 3230–3243. https://doi.org/10.1111/j.1365-2966.2012.22026.x

Pajola, M., Lazzarin, M., Dalle Ore, C. M., Cruikshank, D. P., Roush, T. L., Magrin, S., et al. (2013). Phobos as a D-type captured asteroid, spectral modeling from 0.25 to 4.0 µm. *The Astrophysical Journal*, *777*(2), 127. https://doi.org/10.1088/0004-637X/777/2/127

Pajola, M., Roush, T., Dalle Ore, C., Marzo, G. A., & Simioni, E. (2018). Phobos MRO/CRISM visible and near-infrared (0.5–2.5 µm) spectral modeling. *Planetary and Space Science*, *154*, 63–71. https://doi.org/10.1016/j.pss.2018.02.016

Pajola, M., Simioni, E., Lucchetti, A., Re, C., Cremonese, G., Thomas, N., et al. (2017). Refining the boundary between the Phobos blue/red spectral units with the ExoMars-CaSSIS imagery. *European Planetary Science Congress*, *11*.

Pang, K. D., Pollack, J. B., Veverka, J., Lane, A. L., & Ajello, J. M. (1978). The composition of Phobos: Evidence for carbonaceous chondrite surface from spectral analysis. *Science*, *199*(4324), 64–66. https://doi.org/10.1126/science.199.4324.64

Pang, K. D., Rhoads, J. W., Hanover, G. A., Lumme, K., & Bowell, E. (1983). Interpretation of whole-disk photometry of Phobos and Deimos. *Journal of Geophysical Research*, *88*(B3), 2475–2484. https://doi.org/10.1029/jb088ib03p02475

Patel, M. R., Antoine, P., Mason, J., Leese, M., Hathi, B., Stevens, A. H., et al. (2017). NOMAD spectrometer on the ExoMars trace gas orbiter mission: Part 2—Design, manufacturing, and testing of the ultraviolet and visible channel. *Applied Optics*, *56*(10), 2771–2782. https://doi.org/10.1364/ao.56.002771

Patel, M. R., Pearson, V. K., Evans, D. J., Summers, D. J., Paton, S., Truscott, P., et al. (2019). The transfer of unsterilized material from Mars to Phobos: Laboratory tests, modelling and statistical evaluation. *Life Sciences and Space Research*, *23*, 112–134. https://doi.org/10.1016/j.lssr.2019.08.002

Pieters, C. M., Klima, R. L., Hiroi, T., Dyar, M. D., Lane, M. D., Treiman, A. H., et al. (2008). Martian dunite NWA 2737: Integrated spectroscopic analyses of brown olivine. *Journal of Geophysical Research*, *113*(E6), E06004. https://doi.org/10.1029/2007JE002939

Pieters, C. M., Murchie, S., Thomas, N., & Britt, D. (2014). Composition of surface materials on the moons of Mars. *Planetary and Space Science*, *102*, 144–151. https://doi.org/10.1016/j.pss.2014.02.008

Pieters, C. M., Taylor, L. A., Noble, S. K., Keller, L. P., Hapke, B., Morris, R. V., et al. (2000). Space weathering on airless bodies: Resolving a mystery with lunar samples. *Meteoritics & Planetary Sciences*, *35*(5), 1101–1107. https://doi.org/10.1111/j.1945-5100.2000.tb01496.x

Poggiali, G., Matsuoka, M., Barucci, M. A., Brucato, J. R., Beck, P., Fornasier, S., et al. (2022). Phobos and Deimos surface composition: Search for spectroscopic analogues. *Monthly Notices of the Royal Astronomical Society*, *516*(1), 465–476. https://doi.org/10.1093/mnras/stac2226

Pollack, J. B., Burns, J. A., & Tauber, M. E. (1979). Gas drag in primordial circumplanetary envelopes: A mechanism for satellite capture. *Icarus*, *37*(3), 587–611. https://doi.org/10.1016/0019-1035(79)90016-2

Pollack, J. B., Veverka, J., Pang, K., Colburn, D., Lane, A. L., & Ajello, J. M. (1978). Multicolor observations of Phobos with the Viking Lander cameras: Evidence for a carbonaceous chondritic composition. *Science*, *199*(4324), 66–69. https://doi.org/10.1126/science.199.4324.66

Ramsley, K. R., & Head, J. W. (2017). The Stickney Crater ejecta secondary impact crater spike on Phobos: Implications for the age of Stickney and the surface of Phobos. *Planetary and Space Science*, *138*, 7–24. https://doi.org/10.1016/j.pss.2017.02.004

Ramsley, K. R., & Head, J. W., III. (2013). Mars impact ejecta in the regolith of Phobos: Bulk concentration and distribution. *Planetary and Space Science*, *87*, 115–129. https://doi.org/10.1016/j.pss.2013.09.005

Rivkin, A. S., Brown, R. H., Trilling, D. E., Bell, J. F., III., & Plassmann, J. H. (2002). Near-infrared spectrophotometry of Phobos and Deimos. *Icarus*, *156*(1), 64–75. https://doi.org/10.1006/icar.2001.6767

Roloff, V., Pommerol, A., Gambicorti, L., Servonet, A., Thomas, N., Brändli, M., et al. (2017). On-ground performance and calibration of the ExoMars trace gas orbiter CaSSIS imager. *Space Science Reviews*, *212*(3–4), 1871–1896. https://doi.org/10.1007/s11214-017-0404-2

Ronnet, T., Vernazza, P., Mousis, O., Brugger, B., Beck, P., Devouard, B., et al. (2016). Reconciling the orbital and physical properties of the Martian moons. *The Astrophysical Journal*, *828*(2), 109. https://doi.org/10.3847/0004-637x/828/2/109

Rosenblatt, P., Charnoz, S., Dunseath, K. M., Terao-Dunseath, M., Trinh, A., Hyodo, R., et al. (2016). Accretion of Phobos and Deimos in an extended debris disc stirred by transient moons. *Nature Geoscience*, *9*(8), 581–583. https://doi.org/10.1038/ngeo2742

Simonelli, D. P., Thomas, P. C., Carcich, B. T., & Veverka, J. (1993). The generation and use of numerical shape models for irregular solar system objects. *Icarus*, *103*(1), 49–61. https://doi.org/10.1006/icar.1993.1057

Singer, R. B. (1981). Near-infrared spectral reflectance of mineral mixtures: Systematic combinations of pyroxenes, olivine, and iron oxides. *Journal of Geophysical Research*, *86*(B9), 7967–7982. https://doi.org/10.1029/JB086iB09p07967

Stooke, P. (2015). *Stooke small bodies maps V3. 0*. NASA Planetary Data System, MULTI-SA.

Thomas, N., Cremonese, G., Ziethe, R., Gerber, M., Brändli, M., Bruno, G., et al. (2017). The colour and stereo surface imaging system (CaSSIS) for the ExoMars trace gas orbiter. *Space Science Reviews*, *212*(3–4), 1897–1944. https://doi.org/10.1007/S11214-017-0421-1

Thomas, N., Pommerol, A., Almeida, M., Read, M., Cremonese, G., Simioni, E., et al. (2022). Absolute calibration of the colour and stereo surface imaging system (CaSSIS). *Planetary and Space Science*, *211*, 105394. https://doi.org/10.1016/j.pss.2021.105394

Thomas, P., Veverka, J., Bell, J., Lunine, J., & Cruikshank, D. (1992). Satellites of Mars: Geologic history. In *Mars* (pp. 1257–1282). University of Arizona Press, Space Science Series.

Treiman, A. H., Dyar, M. D., McCanta, M., Noble, S. K., & Pieters, C. M. (2007). Martian Dunite NWA 2737: Petrographic constraints on geological history, shock events, and olivine color. *Journal of Geophysical Research*, *112*(E4), E04002. https://doi.org/10.1029/2006JE002777

Vandaele, A. C., Lopez-Moreno, J. J., Patel, M. R., Bellucci, G., Daerden, F., Ristic, B., et al. (2018). NOMAD, an integrated suite of three spectrometers for the ExoMars trace gas mission: Technical description, science objectives and expected performance. *Space Science Reviews*, *214*(5), 1–47. https://doi.org/10.1007/s11214-018-0517-2

Vilas, F., Gaffey, M. J., Holden, P., & Larson, S. M. (1993). The Soret Band in the spectrum of 2 Pallas. In *American astronomical society, 25th DPS meeting, ID. 36.12-P* (Vol. 25, p. 1135). Bulletin of the American Astronomical Society.

Willame, Y., Depiesse, C., Mason, J. P., Thomas, I. R., Patel, M. R., Hathi, B., et al. (2022). Calibration of the NOMAD-UVIS data. *Planetary and Space Science*, *218*, 105504. https://doi.org/10.1016/J.PSS.2022.105504

Yamada, M., Sasaki, S., Nagahara, H., Fujiwara, A., Hasegawa, S., Yano, H., et al. (1999). Simulation of space weathering of planet-forming materials: Nanosecond pulse laser irradiation and proton implantation on olivine and pyroxene samples. *Earth Planets and Space*, *51*(11), 1255–1265. https://doi.org/10.1186/bf03351599

Zellner, B., & Wells, E. N. (1994). Spectrophotometry of Martian satellites with the Hubble Space Telescope. In *Abstracts of the 25th lunar and planetary science conference, held in Houston, TX* (Vol. 25, p. 1541).